ELSEVIER

Thermochimica Acta 387 (2002) 47–56

thermochimica acta

www.elsevier.com/locate/tca

FINEMET-type nanocrystallization kinetics

Emília Illeková

Institute of Physics SAS, Dúbravská cesta 9, 842 28 Bratislava, Slovak Republic

Received 24 June 2001; received in revised form 10 October 2001; accepted 17 October 2001

Abstract

The primary nanostructure formation kinetics in a set of Fe–Cu–Nb–Si–B ribbons has been studied by the use of differential scanning calorimetry in both continuous-heating and isothermal measuring regimes. The nanostructure formation consists of two independent kinetic modes, namely the Johnson–Mehl–Avrami nucleation-and-growth mode and the mode which has been well described by the normal-grain-growth kinetic law. The nucleation-and-growth of the bcc α-Fe based phase is manifested as a rule in the early stages of the transformation. The normal-grain-growth-like mode is the major and principal kinetic characteristics of all FINEMETs independently of the content of Cu and Si. It is controlled by a specific rearrangement of niobium. After the start of the main nanostructure transformation, a long-range reordering of Si occurs during longer times in the FINEMETs containing Si. $Fe_{75.6}Cu_1Si_{14}B_{9.4}$ is a conventional metallic glass. It does not contain niobium, does not exhibit the normal-grain-growth-like kinetics and does not form the nanocrystalline (FINEMET-type) structure.

Keywords: FINEMET; Nanocrystallization; Kinetics

1. Introduction

Nanostructured materials can be obtained from many conventional metallic glasses by a controlled crystallization at relatively low temperatures. Such nanostructures, however, are in a metastable state and, with sufficiently long annealing time or at high enough temperature, grain growth occurs up to the usual micro-structure grain sizes [1]. The peculiarity of the FINEMET composition [2–4] is that the desired magnetically soft state is supported by a nanocrystalline structure. This structure is relatively stable as a function of annealing time at temperatures between 750 and 850 K owing to the Cu and Nb additions to the Fe–Si–B glass. The formation of a nanostructure in the FINEMET alloy has been found to occur by the primary crystallization of Fe(Si) nanograins (further called the main transformation which represents the first crystallization stage, R1). Above 870 K, the devitrification culminates by the crystallization of the remaining amorphous matrix (the second crystallization stage, R2). The two differential scanning calorimetry (DSC) continuous-heating peaks corresponding to the two stages of crystallization (R1 and R2) were found to be flatter and wider than those corresponding to the related simpler alloy (without Cu and Nb additions). This fact suggests a much slower kinetics of crystallization in the FINEMET (e.g. [5]). It was shown [6] that the dimensions of the primary crystals increase proportionally to the square root of the annealing time. Continuous-heating and isothermal DSC, X-ray, electron microscopy and Mössbauer kinetic analyses, e.g. in [7–11], show that the Johnson–Mehl–Avrami (JMA) law [12] cannot fit the experimental data. Namely, the apparent activation energies for the main transformation, ΔE_1^*, vary with the

0040-6031/02/$ – see front matter
PII: S0040-6031(01)00822-X

measuring regime used from about 143 [8] to 480 kJ mol^{-1} [5]. The JMA exponent, n_1, is approximately equal to unity and even decreases with time, e.g. in [5,7–9]. (The subscript 1 throughout the whole paper relates to the first crystallization stage.)

There are many studies on the crystallization of the $Fe_{73.5}Cu_1Nb_3Si_{13.5}B_9$ alloy and various models are available for the interpretation of its peculiarities. Most frequently, the modification of the residual amorphous matrix caused by the volume diffusion of Si, Cu and/or Nb [13] is assumed to suppress the grain growth rate (e.g. [14]) and eventually to influence the nucleation [15–17] or to interfere with the diffusion fields of neighbor grains [18]. The normal-grain-growth (NGG) kinetics [19,20] was deduced in [9,11]. The participation of more than one kinetic process in the main transformation, R1, in the $Fe_{73.5}Cu_1Nb_3Si_{13.5}B_9$ alloy and in some Si-rich FINEMETs was already assumed in [10,21].

The aim of this paper is to report and interpret the new complex DSC experimental results on the kinetics of the main transformation, R1, in FINEMETs and to relate them to the nanocrystalline structure of their amorphous precursors. A set of alloys with varying Cu content between 0 and 1 at.%, Nb between 0 and 4.5 at.%, and the Si/B ratio between 0 and 1.5 will

Table 1
Thermodynamic and kinetic characterization of the main transformation of the as-cast Fe–Cu–Nb–Si–B ribbons[a]

Sample/chart	Chemical composition	T_a, t_a (K, min)	T_{x1} (K)	T_{p1} (K)	ΔH_1 (J g^{-1})	ΔE_1^* (kJ mol^{-1})	n_1	m_1
$FMCu_0Si_0$	$Fe_{80.5}Nb_7B_{12.5}$							
(1)			788.7	802.7	−20	532 ± 16	no	1
(1_1)		763, 60					1.5	
$FMSi_0$	$Fe_{77.5}Cu_1Nb_{4.5}B_{17}$							
(2)		*	766.9	794.8	−34	*	*	1
$FMSi_{4.5}$	$Fe_{78}Cu_1Nb_3Si_{4.5}B_{13.5}$							
(3)			751.7	765.8	>−61	298 ± 6	no	1
(3_1)		713, 200					2	
(3_2)		723, 60					2	1
(3_3)		813, 60						1
$FMSi_7$	$Fe_{73.5}Cu_1Nb_{3.2}Si_7B_{15.3}$							
(4)		*	809.1	837.7	>−27	600 ± 25	*	1
$FMSi_{9.2}$	$Fe_{74.6}Cu_1Nb_{3.2}Si_{9.2}B_{12}$							
(5)		*	789.8	811.7	>−25	357 ± 33	*	1
$FMCu_0Si_{12.7}$	$Fe_{74.7}Nb_{3.1}Si_{12.7}B_{9.5}$							
(6)			863.6	>873	#	#	#	#
(6_1)		813, 180					4	
$FMSi_{13.5}$	$Fe_{73.5}Cu_1Nb_3Si_{13.5}B_9$							
(7)			815.1	831.4	−45	418 ± 8	no	1.5
(7_1)		778, 60					3	1.5
(7_2)		823, 60					no	no
$FMNb_0$	$Fe_{75.6}Cu_1Si_{14}B_{9.4}$							
(8)			744.3	751.8	−66	314 ± 5	*	no
(8_1)		698, 120					3–1.5	

[a] T_a and t_a are the annealing temperature and time of the isothermal measurements, respectively. T_{x1}, T_{p1} and ΔH_1 are the onset and minimum temperatures and the enthalpy of the continuous-heating DSC peak R1 (heating rate $\beta^+ = 40$ K min^{-1}), respectively. ΔE_1^* is the activation energy deduced by the Kissinger method. n_1 and m_1 (both ± 0.5) are the JMA and NGG exponents deduced by the Suriñach isothermal and continuous-heating methods, respectively. The symbols * and # indicate the quantities which were not or could not be given, respectively.

be presented. The X-ray and electron microscopy characterization of the nanocrystalline structure and the phase analyses of the crystallized samples were already presented in [22–25]. A generalized model of the bimodal JMA-like and NGG-like character of the main transformation in FINEMETs, that we have described first for the $Fe_{73.5}Cu_1Nb_3Si_{13.5}B_9$ alloy in [5,9], will be presented.

2. Experimental

The Fe–Cu–Nb–Si–B glassy ribbons, 10 mm wide and 20–30 μm thick, were prepared by the planar-flow casting technique (the quenching rate $\sim 10^6$ K s^{-1}) in air. The compositions of the materials were checked by the inductively coupled plasma spectroscopy (ICPS) analysis and are shown in Table 1. The samples are further referred to as $FMCu_0Si_0$ up to $FMNb_0$ following Table 1. X-ray diffraction and electron microscopy proved the non-crystalline structure of the samples. The crystallization measurements of as-prepared samples were performed with a Perkin-Elmer DSC7 instrument using a continuous-heating regime from 300 to 873 K with heating rates, β^+, ranging from 5 to 80 K min^{-1} and an isothermal regime with a heating ramp $\beta^+ = 40$ K min^{-1}. The cooling rate was 200 K min^{-1}. The samples were investigated in the as-cast state and also after different in situ pre-annealings at the temperatures ranging from 713 to 823 K. In the case of linear heating, the quasi-linear temperature-variation of the heat capacity of the samples, $C_p(T)$, omitting the Curie point, structural relaxation and crystallization peaks in the first measuring runs and the Curie point in the whole second measuring run, were obtained. Pronounced initial transient effects as well as an additional reaction at $T > 700$ K (probably on the surface of the samples) in both first and second isothermal measuring runs were observed. Therefore, only the first measuring run was always used for the kinetic calculations. The samples were cut into small pieces (10 mg) and covered (not encapsulated) with an Al lid. An empty Al reference pan and flowing argon or nitrogen atmospheres were used.

The absolute temperature (error less that 0.05%) and the enthalpy (error less than 2%) of the DSC instrument were calibrated for all heating rates. The standard calibration materials were In and Zn.

3. Results and discussion

3.1. Dynamic heat treatment

In the main transformation, R1, the nanocrystalline bcc α-Fe is formed in the case of the samples $FMCu_0Si_0$ and $FMSi_0$ (the mean grain size $d < 10$ nm [25]). In other samples, the bcc α-Fe(Si) with increasing tendency to DO_3 ordering with increasing Si content appears [23]. It has a fine-grained structure with the dimensions of the range of nanocrystals in the case of the samples $FMSi_{4.5}$–$FMSi_{13.5}$ ($d \sim 10$ nm [23]). Therefore, all above mentioned samples are further named as FINEMETs. In the sample $FMNb_0$, larger microcrystals ($d > 100$ nm [22]) grow as in the case of conventional metallic glasses.

Fig. 1 shows the details of the continuous-heating main transformation exotherms, R1, of all investigated samples when the heating rate of 40 K min^{-1} is used. The shape of these DSC curves does not depend on the heating rate, β^+. In accordance with the presumption about the thermal activation of the crystallization controlling processes, the exothermal peaks are significantly shifted to higher temperatures with increasing β^+. The R1 peak is wide, asymmetrical, with a long high temperature tail in all samples excepting $FMNb_0$. (In the case of $FMCu_0Si_{12.7}$, the R1 peak occurs above 860 K.)

In all samples, excepting the $FMNb_0$ sample, any pre-annealing at the temperatures below the main transformation shifts the R1 peak to higher temperatures and increases both the onset and minimum peak temperatures, T_{x1} and T_{p1}, respectively. As the end peak temperature, T_{e1}, does not change, the enthalpy decreases in the result as it was shown already for the $FMSi_{13.5}$ sample in Fig. 3 of [5]. Such a peak cannot be represented by any of the conventional JMA crystallization kinetics. On the other hand, it resembles well the NGG kinetics [20]. The above mentioned character of the R1 peaks does not depend on the heating rate, β^+.

In the case of $\beta^+ = 40$ K min^{-1}, the quantitative characteristics of the R1 peaks are summarized in Table 1. The onset and minimum temperatures, T_{x1} and T_{p1}, respectively, vary with the actual chemical composition. They are significantly higher in the samples without Cu. All main transformation enthalpies,

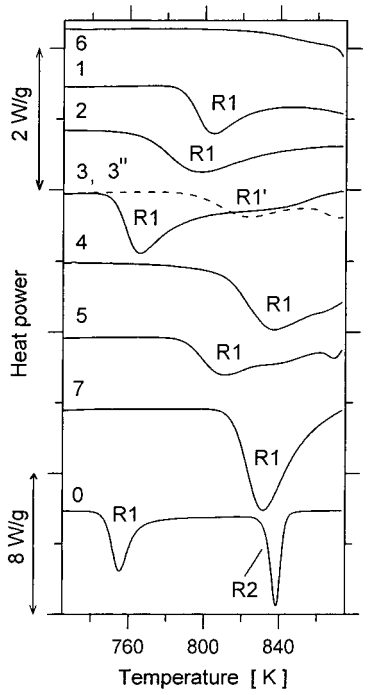

Fig. 1. Continuous-heating DSC signal from the main transformation process of various as-cast Fe–Cu–Nb–Si–B ribbons. 1—$FMCu_0Si_0$, 2—$FMSi_0$, 3—$FMSi_{4.5}$ (dashed line 3″ refers to the isothermally pre-annealed at 713 K for 200 min sample), 4—$FMSi_7$, 5—$FMSi_{9.2}$, 6—$FMCu_0Si_{12.7}$, 7—$FMSi_{13.5}$, 8—$FMNb_0$. The chemical compositions of the samples are in Table 1. The crystallization stages R1, R1′ and R2 are related to the DSC exothermal peaks for some samples. The heating rate is 40 K min^{-1}. The vertical scale for the sample $FMNb_0$ (curve 8) is shrunk by the factor of 4.

ΔH_1, are less than one-half of the enthalpy of the first crystallization peak of the $Fe_{75}Si_{15}B_{10}$ metallic glass (104 J g^{-1} in [26]). These quantities are also proportional to the content of the crystallized product. The main transformation activation energies, ΔE_1^* (calculated from the β^+ dependence of T_p [27]), are less significant because of their dependence on the heat treatment of the samples and the disagreement with related quantities calculated by other methods (see e.g. [5]). In addition, another minor transformation stage, R1′, occurs before the termination of R1 peaks which is accompanied by changes of magnetic properties and grain dimensions in the samples containing Si. Its separation by isothermal heat treatment is demonstrated in Fig. 1 in the case of the sample $FMSi_{4.5}$. A similar effect has already been observed previously for the sample $FMSi_{13.5}$ [5]. At higher temperatures, the second complex exothermal peak, R2, always follows due to the grain growth and the crystallization of the remaining amorphous matrix [22].

3.2. Isothermal heat treatment

In the isothermal experiments, the samples were heated up to the transformation temperature, $T_{x1} - 50\,K < T_a < T_{x1}$, ($\beta^+ = 40$ K min^{-1}) and kept at T_a until the signal was saturated. After cooling down to room temperature, the samples were measured again either in the isothermal or continuous-heating regimes. In both cases, the DSC signal gave just the transient instrument effect followed by a baseline (details for the sample $FMSi_{13.5}$ see e.g. in [5]).

The isothermal main transformation "exotherms" have a bimodal character (Fig. 2) for all FINEMET-type samples. The DSC signal after a steep negative

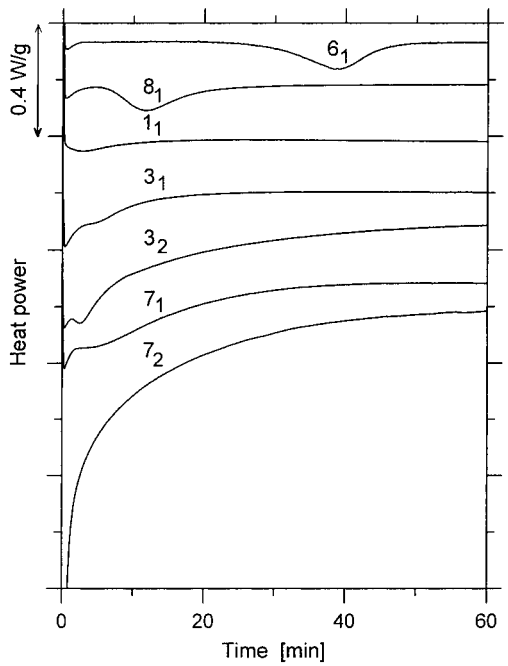

Fig. 2. Isothermal DSC traces from the main transformation process of various as-cast Fe–Cu–Nb–Si–B alloys. 6_1—$FMCu_0Si_{12.7}$ (813 K), 8_1—$FMNb_0$ (698 K), 1_1—$FMCu_0Si_0$ (763 K), 3_1—$FMSi_{4.5}$ (713 K), 3_2—$FMSi_{4.5}$ (723 K), 7_1—$FMSi_{13.5}$ (778 K), 7_2—$FMSi_{13.5}$ (823 K). The chemical compositions of the samples are in Table 1.

increase either monotonically decreases (curve 7_2), suggesting the NGG kinetics [20], or a conventional JMA exothermal peak is measured (curves 6_1 and 8_1). Usually, both effects act simultaneously (curves 3_1, 3_2 and 7_1). The mutual relation between both effects is strongly dependent on temperature due to a typical T_a dependence of the peak mode suggesting the JMA kinetics whereas the decay effect is relatively insensitive to T_a (see curves 3_1 and 3_2 for the sample $FMSi_{4.5}$). At lower temperatures, $T_a \sim T_{x1} - 50$ K, only the peak mode was detected (curve 6_1) whereas at higher temperatures, $T_a > T_{x1} - 10$ K, only the decay mode could be detected (curve 7_2). Besides, the enthalpic proportion between the NGG-like and JMA-like modes is strongly related to the chemical composition of the samples.

3.3. Kinetic analysis

As it was found, the classical JMA kinetic laws fail in the case of the continuous-heating main transformation of FINEMETs. Besides, the same crystallization stage reveals the bimodal character in the isothermal regime. Therefore, the Suriñach curve fitting procedure [28,29] might specify the complex character of the R1 stage. In this way, each single DSC curve (dynamic or isothermal), represented in an appropriate coordination system, namely

$$\ln\left[\frac{\mathrm{d}\alpha(T,t)}{\mathrm{d}T}\right] + \frac{\Delta E^*}{[RT(t)]} + \ln\beta^+ \quad \text{versus} \quad -\ln[1-\alpha(T,t)] \tag{1}$$

or

$$\ln\left[\frac{\mathrm{d}\alpha(T,t)}{\mathrm{d}t}\right] + \frac{\Delta E^*}{(RT_a)} \quad \text{versus} \quad -\ln[1-\alpha(T,t)] \tag{2}$$

is compared with the theoretical ones. Here, $\mathrm{d}\alpha(T,t)/\mathrm{d}T$ and $\mathrm{d}\alpha(T,t)/\mathrm{d}t$ are directly proportional to the DSC continuous-heating and isothermal signal, respectively, where $(\mathrm{d}\alpha/\mathrm{d}T) = (1/\Delta H\beta^+)(\mathrm{d}H/\mathrm{d}t)$ and $\mathrm{d}\alpha/\mathrm{d}t = (1/\Delta H)(\mathrm{d}H/\mathrm{d}t)$, α and R being the degree of transformation and the gas constant, respectively. Theoretically possible R1 stage kinetic laws are described in Table 2 and their Suriñach curves are shown in Fig. 3, namely the conventional JMA kinetics, the NGG kinetics, that is insinuated both in the continuous-heating and isothermal measurements, and the diffusion that is supposed to participate by some authors.

Table 2
Theoretical kinetic model equations [19,28] considered

Equation	$\mathrm{d}\alpha/\mathrm{d}T$	Label
Johnson–Mehl–Avrami	$(1-\alpha)\{-\ln(1-\alpha)\}^{(n-1)/n}$	n
Normal–grain–growth	$(1-\alpha)^{m+1}$	m
Three-dimensional diffusion	$[(1-\alpha)^{-1/3}-1]^{-1}$	d

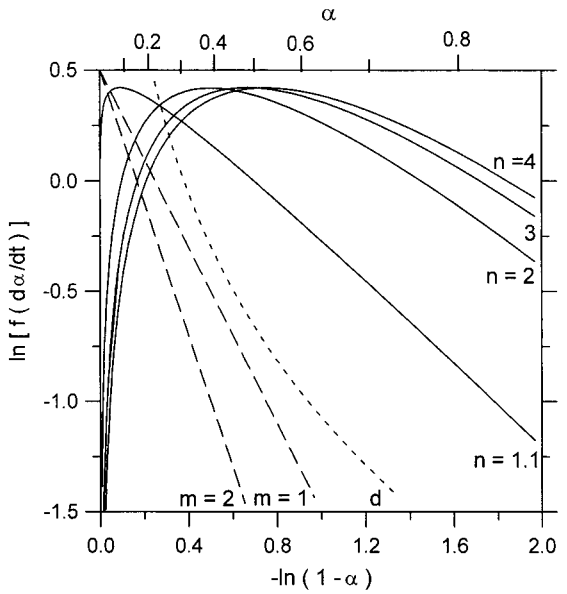

Fig. 3. Suriñach plots [28] for the different theoretical kinetic equations summarized in Table 2. Full lines correspond to the JMA kinetics, exponent n being the parameter. The dashed line corresponds to the NGG kinetics, exponent m being the parameter. The dotted line corresponds to the three-dimensional diffusion kinetics. The JMA model lines are shifted to show the maxima at the same level.

In the case of the DSC continuous-heating R1 peaks, the Suriñach representation and the least-squares minimization procedure were utilized. All peaks from Fig. 1 as well as the thermograms taken at all heating rates were used. It was found that the kinetics of the R1 stage follows one characteristic master curve for all as-cast samples except the sample $FMNb_0$ as it can be seen in Fig. 4. Using the curve fitting procedure, the kinetics were specified. Namely, the main transformation begins with the JMA-like kinetics having the JMA exponent $1 < n_1 < 1.5$. Next, it decays quickly and the master curve is parallel

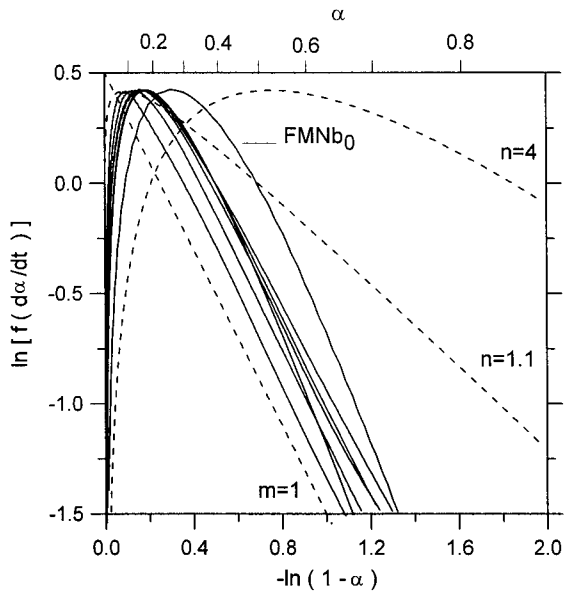

Fig. 4. Suriñach representations of the continuous-heating DSC curves in Fig. 1 from the main transformation of as-cast Fe–Cu–Nb–Si–B ribbons. The $FMNb_0$ sample is marked. The curves are shifted to show the maxima at the same level. Dashed lines are the plots for the theoretical JMA kinetics with $n = 4$ and 1.1 and NGG kinetics with $m = 1$.

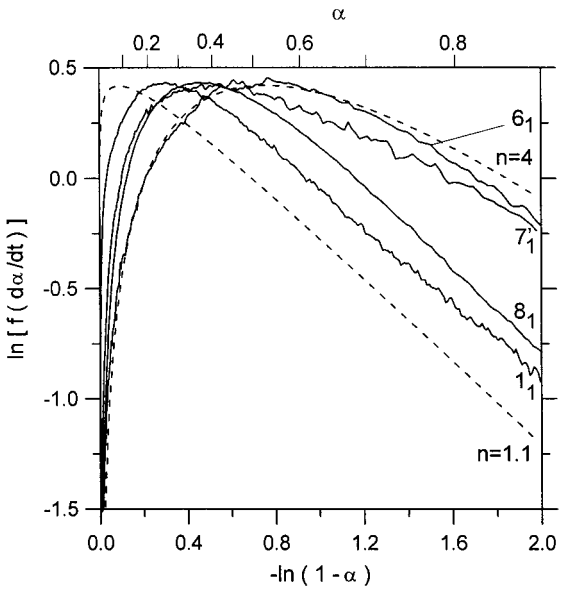

Fig. 5. Suriñach representations of the JMA-like mode in the main transformation of some as-cast Fe–Cu–Mn–Si–B ribbons taken from the separated isothermal DSC peaks in Fig. 2. 6_1—$FMCu_0Si_{12.7}$ (813 K), 8_1—$FMNb_0$ (698 K), 1_1—$FMCu_0Si_0$ (763 K), $7'_1$—$FMSi_{13.5}$ (778 K) separated peak only. The chemical compositions of the samples are in Table 1. The curves are shifted to show the maxima at the same level. Dashed lines are the plots for the theoretical JMA kinetics with $n = 4$ and 1.1.

to the NGG-like theoretical straight line with the NGG exponent $m_1 \geq 1$ for $\alpha_1 \geq 0.2$. The variability of the chemical composition of the FINEMETs has no principal influence on the master curve. Concerning the reliability of the Suriñach analysis, the uncertainty of the ΔE_1^*, values (see Table 1) influenced the Suriñach plots within 10%. The Suriñach plots deformation due to the participation of R1′ process in the advanced stages of R1 was not significant. The incompleteness of some R1 peaks shifted the Suriñach plots to the right side. The interpretation of the kinetics of the sample $FMNb_0$ is not clear. Its Suriñach plot implies a significantly higher proportion of the JMA-like kinetic mode with n_1 decreasing from 2.5 to 1.5 for $\alpha_1 < 0.3$. Then, the curve is gradually degraded due to the presence of the R2 crystallization stage ($T_{x1} - T_{x2} = 84.6$ K). The NGG-like mode was not detected in this case.

In the case of the DSC isothermal FINEMET's bimodal main transformation curves (Fig. 2), the JMA-like mode (the peak) might be separated from the NGG-like mode (the decay) by the appropriate baseline subtraction. This was done for the curves 3_2 and 7_1 and the straight-line baseline was used. Figs. 5 and 6 show the Suriñach representation of the subtracted peaks. In the case of the sample $FMCu_0Si_{12.7}$, the nearly perfect JMA-like kinetics with $n_1 = 4$ is deduced (curve 6_1 in Fig. 5). $n_1 = 1.5$ for the sample $FMCu_0Si_0$ (curve 1_1 in Fig. 5). Concerning the other curves, the fits as well as the sophisticated JMA exponents are not ideal also due to the relatively low partial enthalpy being analyzed. However, the JMA-like kinetics is always unambiguously demonstrated. The JMA exponents vary between 3 and 1.5, e.g. n_1 decreases in the case of the sample $FMNb_0$ (curve 8_1 in Fig. 5) and increases in the case of the sample $FMSi_{13.5}$ (curve $7'_1$ in Fig. 5) with the annealing time.

In Fig. 6, our hypothesis of the participation of several independent processes in the first crystallization stage in FINEMETs (two modes of the main transformation, R1, and the participation of the R1′ stage) is evidenced and the influence of this fact on the deduced kinetic laws for the deconvoluted individual

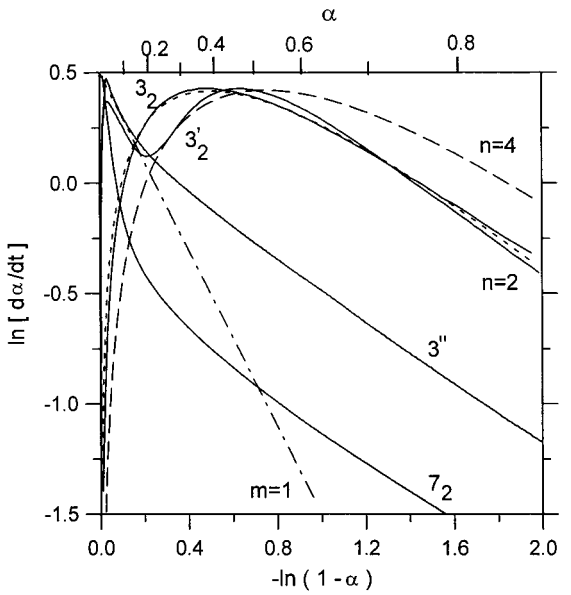

Fig. 6. The Suriñach plots showing the difference between the JMA-like and NGG-like modes in the main transformation of the as-cast Fe–Cu–Nb–Si–B ribbons. The isothermal data are taken from Fig. 2. 3_2—$FMSi_{4.5}$ (723 K), $3'_2$—$FMSi_{4.5}$ (723 K) separated peak only, 7_2—$FMSi_{13.5}$ (823 K). $3''$—the continuous-heating run of isothermally pre-annealed at 713 K for 200 min $FMSi_{4.5}$ sample (data are from Fig. 1). The chemical compositions of the samples are in Table 1. Dashed lines are the plots for the theoretical JMA kinetics with $n = 4$ and 2 and NGG kinetics with $m = 1$. The curves are shifted to show the JMA maxima at the same level.

processes is demonstrated. The dashed lines represent the theoretical model JMA kinetics (with $n = 2$ and 4) and the NGG kinetics (with $m = 1$). In the case of the sample $FMSi_{4.5}$ (curve 3_2 in Fig. 2), the Suriñach plot follows the NGG-like kinetics for $\alpha_1 < 0.2$, then the kinetics continuously changes (when the peak starts to appear in the DSC signal) fitting well the JMA-like one with $n_1 = 3$ and finally with $n_1 = 2$ for $\alpha_1 > 0.5$ (see curve 3_2 in Fig. 6). On the other hand, the Suriñach plot of the subtracted peak (from the same curve 3_2 in Fig. 2) fits only one mode having the JMA kinetics with $n_1 = 2$ for all α_1 (see curve $3'_2$ in Fig. 6). The same holds also true for slightly modified T_a (e.g. for the curve 3_1 in Fig. 2) as well as for the other samples. However, in the case of sufficiently high annealing temperatures, $T_a > T_{x1} - 10$ K the decay mode is only observed (curve 7_2 in Fig. 2) and the Suriñach plot starting with the NGG-like kinetics finally shows the concave curvature (see curve 7_2 in Fig. 6). This indicates the long-range diffusion (as in the case of the theoretical curve d in Fig. 3). Also in the case of R1′ stage, no JMA-like kinetics and significant contributions of the long-range diffusion kinetics are indicated (curve $3''$ in Fig. 6).

In the case of the isothermal main transformation DSC curves in Fig. 2, also the JMA curve fitting procedure [12] can be formally applied and the results deduced from the Suriñach kinetic analysis have to be confirmed. Thus, in the case of the conventional crystallization, the JMA exponent n is the slope of the

$$\ln(-\ln[1-\alpha(T,t)]) \quad \text{versus} \quad \ln(t-\tau_{JMA}) \tag{3}$$

dependence where τ_{JMA} is a linearization parameter which can be received from the least-square minimization fitting procedure of the difference between the measured (3) and simulated points (linear dependence). The JMA analysis (Fig. 7) has shown $n_1 = 4$ after the incubation time $\tau_{JMA} = 220$ s in the case of the sample $FMNb_0$. The JMA exponent decreases to $n_1 = 1.5$ in the advanced stages of the isothermal crystallization DSC peak for $\alpha_1 > 0.6$ (curve 8_1). The linear plateau of the JMA plots is narrower and $n_1 = 3$ at relatively low T_a after $\tau_{JMA} = 2470$ s in the sarnple $FMCu_0Si_{12.7}$ (curve 6_1). In the case of the bimodal DSC curves even if the peak mode was separated from the decay mode by the subtraction procedure, the slope of the JMA shows a systematic artificial decrease from 4 to 3 and finally to 1.5 as in the case of the samples $FMSi_{13.5}$ and $FMSi_{4.5}$ (curves $7'_1$ and $3'_2$). In the case of the sample $FMCu_0Si_0$, $n_1 = 1.5$ for $0.02 < \alpha_1 < 0.63$ (curve 1_1). If we suppose that the peak mode provided a less significant contribution and therefore could not be separated, the JMA curve after the initial $n_1 = 1.5$ gives a broad plateau with $n_1 \sim 1$ in the case of the sample $FMSi_{4.5}$ (curve 3_1). Otherwise, the slope of the JMA plot rapidly decreases after a short time giving an extremely low exponent $n_1 < 1$ as at high T_a in the case of the sample $FMSi_{13.5}$ (curve 7_2). The last mentioned case is the most frequent and characteristic one in the case of the FINEMETs.

4. Interpretation

On the basis of both continuous-heating and isothermal DSC measurements and the complex kinetics

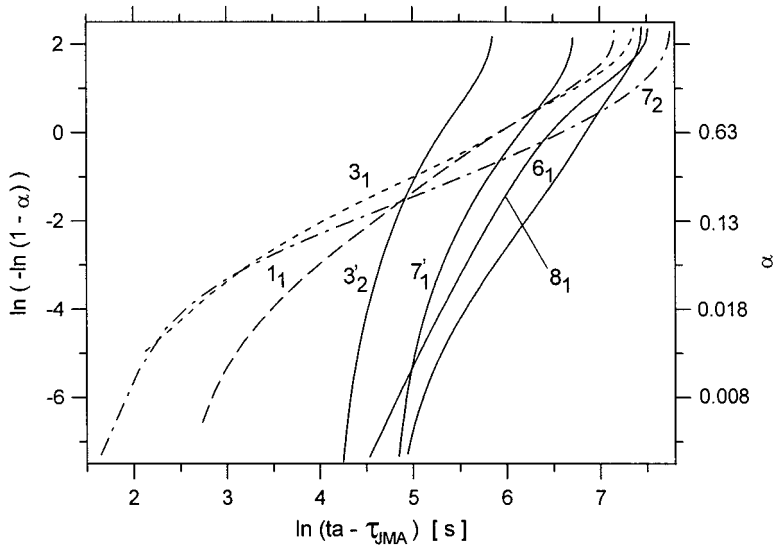

Fig. 7. Linearized JMA representation of the isothermal DSC traces in Fig. 2 from the main transformation of various as-cast Fe–Cu–Nb–Si–B ribbons. 6_1—$FMCu_0Si_{12.7}$ (813 K), 8_1—$FMNb_0$ (698 K), 7_1—$FMSi_{13.5}$ (778 K) separated peak only, 3_2—$FMSi_{4.5}$ (723 K) separated peak only, 1_1—$FMCu_0Si_0$ (763 K), 3_1—$FMSi_{4.5}$ (713 K), 7_2—$FMSi_{13.5}$ (823 K). The chemical compositions of the samples are in Table 1.

analysis, the model of the crystallization of the FINEMETs is proposed. The main transformation of FINEMETs (R1 stage) is composed of two processes, namely the JMA-like and the NGG-like ones. These two modes are mutually independent.

The JMA-like mode represents both the nucleation and the three dimensional crystal growth of the bcc α-Fe-based phase in the amorphous precursor. As a rule, it takes part at lower temperatures or at the beginning of R1. The JMA exponent, n_1, initially beings at 4 for the samples rich in Si and continuously decreases to 1.5 with decreasing Si content. The nucleation saturates and the initially interface reaction controlled growth tends to be diffusion controlled with increasing temperature and annealing time. Both the occurrence and the decay of the nucleation processes might by assumed relying, e.g. on the measurements of the particle size distribution of Fe(Si) crystallites in Si and Cu containing FINEMETs in [30]. The results in [17] suggest that a coarsening of Cu clusters occurs in another exothermal event prior to the heterogeneous nucleation of Fe(Si) primary crystals. Three-dimensional crystal growth process is supported by the spherulitic shape of the nanocrystals in the samples, [22,23]). The JMA-like mode takes place in all samples under study.

The NGG-like kinetics is the most characteristic feature of the FINEMET's kinetics. It takes part in a wide temperature range dominating at higher temperatures and in the advanced stages of R1. The spontaneous main transformation of FINEMETs due to the continuous-heating regime is represented solely by the NGG-like mode. NGG-like mode is related neither to the presence of Si (see the sample $FMSi_0$) nor to the presence of Cu (see the sample $FMCu_0Si_0$) in the samples. It is not necessarily related to the existence of the nanocrystalline product as it was shown in the case of FINEMETs enriched by more than 20 at.% of Ni [31]. (The $Fe_{53.5}Ni_{20}Cu_1Nb_3Si_{13.5}B_9$ samples were nanocrystalline, nevertheless, they did not show the NGG-like kinetics). The NGG-like kinetics was not detected in the samples without Nb (the sample $FMNb_0$). Therefore, a relation between the transport of Nb in the Fe–(Si)–B amorphous matrix and the NGG-like kinetics may be presumed. (Similar indirect conclusions might be done from the observations of Naohara, see Figs. 2 and 3 in [32] for Fe–Si–B samples containing at least 3 at.% of Nb. The crystal growth controlled by niobium diffusion assumed also Köster et al. in [6].)

After the start of R1, another independent process, R1 , also takes part during the longer times in FINEMETs containing Si. It occurs at higher temperatures starting at T_{x1} 793 K for $FMSi_{4.5}$ and T_{x1} 880 K for $FMSi_{13.5}$. For R1 , the diffusion

kinetics is deduced which well correlates with the electron microscopy observations of the long-range reordering of Si in the bcc α-Fe(Si) phase in [23].

Although the kinetics of the main transformation in FINEMETs is characterized by always the same NGG-like master curve, related mechanisms can hardly be accepted. The driving force for the NGG process is the decrease of the interfacial enthalpy of the sample which is assumed to be related to the measured DSC signal [19]. The conventional idea of the mechanism [19], where larger grains in the already fine-crystalline sample increase their size at the expense of smaller ones, does not correlate with the structural observations in our case. Two modifications need to be taken into account at least. The first one should reflect the presence of two dispersed amorphous phases [33,34] where only one undergoes the transformation. The second one should be related to the specific role of niobium. Further new mechanisms might be found in terms of the cluster model of Hamada and Fujita [35] or of the coupled fluxes model of Kelton [36].

Hermann et al. [30] proposed a theoretical approach to the crystallization kinetics which takes into account the influence of microstructure and microstructural changes during crystallization. A certain critical radius of as-created nuclei and slowly diffusing nhibitors were found to be the controlling parameters of the evolution of the individual crystallites in this model. The authors derived a multiparameter integral equation which could describe isothermal main transformation data of some FINEMETs (the NGG-like mode in the case of our isothermal data). In [37] it was experimentally evidenced that the accumulated Nb atoms or Nb–B aggregates could act as inhibitors at the surface of nanocrystalites in FINEMETs.

A mutual relation between the JMA-like and NGG-like mechanisms has to be examined, too. The characterization of the mechanisms satisfying both the structural and kinetic peculiarities of FINEMETs will be the subject of our next studies.

5. Conclusions

This paper deals with the transformation kinetics of Fe–Cu–Nb–Si–B alloys from the as-cast amorphous state to the nanocrystalline state. DSC in the continuous-heating and isothermal regimes were used for the measurements. The Suriñach curve fitting procedure was used for the analysis. The following results were obtained.

1. The continuous-heating main transformation, R1, (the exothermal peak) kinetics of all FINEMET-type alloys follows one master curve. The shape of the curve as well as its heat-treatment dependence cannot be interpreted by any of the conventional JMA crystallization kinetics. The data correlate well with the theoretical NGG kinetic law with the NGG exponent m_1 1.
2. The isothermal main transformation kinetics of the FINEMET-type alloys has a bimodal character. The proportion between the JMA-like and the NGG-like modes is related to the temperature and chemical composition of the samples.

Relying on all observed facts, the following kinetic model is concisely formulated.

1. The nanostructure formation of any FINEMET-type sample is composed of the processes of two types, namely the Johnson–Mehl–Avrami nucleation-and-growth mode and the mode which has been well described by the normal-grain-growth kinetic law. These two modes are mutually independent.
2. The nucleation-and-growth kinetics is manifested as a rule in the early stages of the R1 transformation. It represents both the nucleation and the three-dimensional crystal growth of the bcc α-Fe-based phase which is dispersed in the amorphous matrix. The JMA exponent, n_1, initially begins at 4 for the samples rich in Si and continuously decreases to 1.5 by increasing the time of the thermal treatment.
3. The normal-grain-growth-like mode dominates at higher temperatures and in the advanced stages of the R1 transformation. It is independent of the content of Cu and Si and is controlled by the specific rearrangement of niobium. If the NGG-like kinetics takes place in an initially amorphous sample, the nanocrystalline structure must be formed.
4. The $Fe_{75.6}Cu_1Si_{14}B_{9.4}$ sample does not exhibit the NGG-like kinetics and does not form the nanocrystalline (FINEMET-type) structure.

5. After the start of the R1 transformation, the long-range diffusion of Si controlled reordering (the R1 transformation) takes part during longer times in the FINEMETs containing Si.

Acknowledgements

The author is grateful to Dr. P. Duhaj for the preparation of the metallic ribbons. The work was supported by the Slovak Scientific Grant Agency VEGA under the Grants no. 2/6064/99 and 2/6065/99.

References

[1] L.K. Varga, É. Bakos, L.F. Kiss, I. Bakonyi, Mater. Sci. Eng. A 180 (1994) 567.
[2] Y. Yoshizawa, S. Oguma, K. Yamauchi, J. Appl. Phys. 64 (1988) 6044.
[3] Y. Yoshizawa, K. Yamauchi, T. Yamana, H. Sugihara, J. Appl. Phys. 64 (1988) 6047.
[4] G. Herzer, in: K.H.J. Busehow (Ed.), Handbook of Magnetic Materials, Vol. 10, Vacuumschmelze GmbH, Elsevier, 1997 (Chapter 3).
[5] E. Illeková, K. Czomorová, F.A. Kuhnast, J.M. Fiorani, Mater. Sci. Eng. A 205 (1996) 166.
[6] U. Köster, U. Schünemann, M. Blank-Bewersdorff, S. Brauer, M. Sutton, G.B. Stephenson, Mater. Sci. Eng. A 133 (1991) 611.
[7] G. Hampel, A. Pundt, J. Hesse, J. Phys.: Condens. Matter 4 (1992) 3195.
[8] A. Cserei, J. Jiang, F. Aubertin, U. Gonser, J. Mater. Sci. 29 (1994) 1213.
[9] E. Illeková, F.A. Kuhnast, J.M. Fiorani, Nanostructured and non-crystalline materials, in: M. Vázquez, A. Hemando (Eds.), Proceedings of the 4th International Workshop on Non-Crystalline Solids, Madrid, Spain, 20–23 September 1994, World/Scientific, Singapore, 1995, p. 490.
[10] N. Clavaguera, M.T. Clavaguera-Mora, J. Zhou, F. de Beurmann, Nanostructured and non-crystalline materials, in: M. Vázquez, A. Hernando (Eds.), Proceedings of the 4th International Workshop on Non-Crystalline Solids, Madrid, Spain, 20–23 September 1994, World/Scientific, Singapore, 1995, p. 510.
[11] N. Lécaudé, J.C. Perron, JMMM 160 (1996) 263.
[12] J.W. Christian, The Theory of Transformations in Metals and Alloys, Pergamon Press, Oxford, 1975.
[13] K. Hono, A. Inoue, T. Sakurai, Appl. Phys. Lett. 58 (1991) 2180.
[14] J.Z. Jiang, Nanostructured Mater. 9 (1997) 245.
[15] J.D. Ayers, V.G. Harris, J.A. Sprague, W.T. Blam, Appl. Phys. Lett. 64 (1994) 974.
[16] A.R. Yavari, D. Negri, Mater. Sci. Forum 307 (1999) 63.
[17] M. Ohnuma, K. Hono, S. Linderoth, J.S. Pedersoen, Y. Yoshizawa, H. Onodera, Acta Mater. 48 (2000) 4783.
[18] D. Crespo, T. Pradell, M.T. Clavaguera-Mora, N. Clavaguera, Phys. Rev. B 55 (1997) 3435.
[19] H.V. Atkinson, Acta Metall. 36 (1988) 469.
[20] L.C. Chen, F. Spaepen, J. Appl. Phys. 69 (1991) 679.
[21] N. Lécaudé, J.C. Perron, Mater. Sci. Forum 269–272 (1998) 713.
[22] P. Duhaj, P. Švec, D. Janičkovič, I. Mat'ko, M. Hlásnik, Mater. Sci. Eng. B 14 (1992) 357.
[23] P. Duhaj, P. Švec, I. Mat'ko, D. Janičkovič, Key Eng. Mater. 81–83 (1993) 39.
[24] B. Idzikowski, J. Baszyński, I. Škorvańek, K.H. Müller, D. Eckert, J. Magn. Magn. Mater. 177–181 (1998) 941.
[25] J. Marcin, A. Wiedenmaun, I. Škorvańek, Phys. B 276–278 (2000) 870.
[26] E. Illeková, I. Mat'ko, P. Duhaj, F.A. Kuhnast, J. Mater. Sci. 32 (1997) 4645.
[27] H.E. Kissinger, Anal. Chem. 29 (1957) 1702.
[28] S. Suriñach, M.D. Baró, M.T. Clavaguera-Mora, N. Clavaguera, J. Non-Cryst. Solids 58 (1983) 209.
[29] B. Illeková, Thermochim. Acta 280/281 (1996) 289.
[30] H. Hermann, N. Mattern, S. Roth, P. Uebele, Phys. Rev. B 56 (1997) 13888.
[31] B. Illeková, P. Duhaj, Acta Phys. Slov. 50 (2000) 525.
[32] T. Naohara, Acta Mater. 46 (1998) 397.
[33] J.M. Dubois, G. Le Caer, Nucl. Instr. Methods 199 (1982) 307.
[34] I. Mat'ko, E. Illeková, P. Švec, P. Duhaj, Mater. Sci. Eng. A 225 (1997) 145.
[35] T. Hamada, F.E. Fujita, Jpn. J. Appl. Phys. 21 (1982) 981.
[36] K.F. Kelton, J. Non-Cryst. Solids 274 (2000) 147.
[37] H. Hermann, A. Heinemann, N. Mattern, A. Wiedenmann, Europhys. Lett. 51 (2000) 127.